Keratinocyte-Derived Exosomes in Painful Diabetic Neuropathy

Authors: James Coy-Dibley[1], Nirupa D. Jayaraj[1], Dongjun Ren[2], Paola Pacifico[1], Abdelhak Belmadani[1, 2], Yi-Zhi Wang[1], Kamil K. Gebis[1], Jeffrey N. Savas[1], Amy S. Paller[3], Richard J. Miller[2], Daniela M. Menichella[1, 2]^.

Author affiliation: [1]Department of Neurology, Feinberg School of Medicine, Northwestern University, Chicago, IL, USA, [2]Department of Pharmacology, Feinberg School of Medicine, Northwestern University, Chicago, IL, USA. [3]Department of Dermatology, Feinberg School of Medicine, Northwestern University, Chicago, IL, USA

^ Corresponding author: Daniela Maria Menichella

James Coy-Dibley, MFA

Conflict of interest statement: The authors have declared that no conflict of interest exists.

ABSTRACT

Painful diabetic neuropathy (PDN) is a challenging complication of diabetes with patients experiencing a painful and burning sensation in their extremities. Existing treatments provide limited relief without addressing the underlying mechanisms of the disease. PDN involves the gradual degeneration of nerve fibers in the skin. Keratinocytes, the most abundant epidermal cell type, are closely positioned to cutaneous nerve terminals, suggesting the possibility of bi-directional communication. Exosomes are small extracellular vesicles released from many cell types that mediate cell to cell communication. The role of keratinocyte-derived exosomes (KDEs) in influencing signaling between the skin and cutaneous nerve terminals and their contribution to the genesis of PDN has not been explored. In this study, we characterized KDEs in a well-established high-fat diet (HFD) mouse model of PDN using primary adult mouse keratinocyte cultures. We obtained highly enriched KDEs through size exclusion chromatography and then analyzed their molecular cargo using proteomic analysis and small RNA sequencing. We found significant differences in the protein and microRNA content of HFD KDEs compared to KDEs obtained from control mice on a regular diet (RD), including pathways involved in axon guidance and synaptic transmission. Additionally, using an *in vivo* conditional extracellular vesicle (EV) reporter mouse model, we demonstrated that epidermal-originating GFP-tagged KDEs are retrogradely trafficked into the DRG neuron cell body. Overall, our study presents a potential novel mode of communication between keratinocytes and DRG neurons in the skin, revealing a possible role for KDEs in contributing to the axonal degeneration that underlies neuropathic pain in PDN. Moreover, this study presents potential therapeutic targets in the skin for

47 developing more effective, disease-modifying, and better-tolerated topical interventions
48 for patients suffering from PDN, one of the most common and untreatable peripheral
49 neuropathies.

50 **INTRODUCTION**

51 Diabetes Mellitus is a very prevalent disease with 29.3 million adults living with
52 diabetes and 115.9 million with pre-diabetes[1]. Painful diabetic neuropathy (PDN) is a
53 disabling, intractable, and common syndrome occurring in approximately 25% of
54 diabetics[2-5]. The associated neuropathic pain significantly impacts the quality of life for
55 patients[6]. Despite its prevalence and impact, current therapies for PDN have limited
56 effects in treating pain[7-10], fail to remediate the damage to nerves, and have side effects
57 associated with their systemic administration[10-12]. Therefore, there is an urgent need for
58 better tolerated and more effective therapies for PDN.

59 PDN is characterized by neuropathic pain associated with dorsal root ganglion
60 (DRG) nociceptor hyperexcitability and the degeneration of the DRG neuron axons that
61 innervate the skin[13,14]. This results in small fiber neuropathy, where there is a loss or
62 retraction of the cutaneous nerves in the skin epidermis[13,14]. A critical barrier to
63 developing effective treatments for PDN is the lack of understanding of the molecular
64 mechanisms leading to neuropathic pain and small fiber neuropathy.

65 Keratinocytes are the most abundant epidermal cell type. Recent studies have
66 discovered a new role for keratinocytes in mediating innocuous and noxious touch and
67 thermal sensation in healthy skin[15]. Keratinocytes detect touch stimuli in the skin and
68 transmit mechanical information related to pressure and brushing[16,17]. Optogenetic
69 inhibition of keratinocytes *in vivo* inhibits the responses to noxious mechanical and
70 thermal stimuli[17,18]. There is also evidence that keratinocytes may contribute to persistent
71 neuropathic pain. A study involving the transplantation of human keratinocytes into
72 rodents with transected nerves showed increased excitability of DRG neurons and

73 chronic pain *in vivo*[19]. However, the specific role of keratinocytes in PDN has not been
74 widely investigated.

75 The skin is a highly complex biological system. Along with nociceptive DRG
76 neurons, various other neuronal subpopulations terminate in the skin, both in the dermis
77 and the epidermis[5]. Keratinocytes are closely juxtaposed to cutaneous nerve terminals,
78 suggesting that there may be bidirectional communication. Interestingly, in rodents and
79 human skin, cutaneous nerve terminals in the epidermis form synapse-like contacts and
80 also tunnel through keratinocytes, where they form connexin-43 positive gap junctions,
81 enabling direct cellular communication[20,21]. However, the functional implications of such
82 observations remain unclear. One such ubiquitous mode of intercellular communication
83 recently garnering more appreciation in the skin is mediated by extracellular vesicles
84 (EVs).

85 Exosomes, which are small EVs composed of lipids, proteins and nucleic acids[22-
86 25], were initially posited to be involved in removing cellular waste[26]. However, a substantial
87 body of research now suggests a wider role in intercellular communication. Exosomes
88 are released from most cell types and have been linked to several neurogenerative
89 diseases[27,28] and the progression of different cancers[29]. Keratinocyte-derived exosomes
90 (KDEs) have demonstrated their ability to modulate melanocyte pigmentation[30], regulate
91 dermal fibroblast gene expression[31], mediate crosstalk with macrophages in cutaneous
92 wound healing[32] and play a crucial role in dermal immune responses in psoriasis [33,34].
93 And it has been demonstrated that EVs derived from mesenchymal stem cells can directly
94 alter the excitability of DRG nociceptors in mice[35]. The exploration of the role of exosomes
95 in diabetes, however, has primarily focused on adipose tissue and interorgan

96 communication[36-38]. Recent studies have unveiled a potential role for exosomes in
97 impaired wound healing associated with diabetes[39]. Yet, the research on the effects of
98 exosomes on diabetic neuropathy is limited and has been conducted using exosomes
99 isolated from mesenchymal cells[40,41] or Schwann cells[42]. Notably, exosomes isolated from
100 mesenchymal stromal cells have shown promise in ameliorating peripheral neuropathy in
101 a mouse model of diabetes[40]. Conversely, exosomes derived from high glucose-
102 stimulated Schwann cells have been found to promote the development of diabetic
103 neuropathy in mice[42]. A rigorous and comprehensive investigation of keratinocyte-derived
104 exosomes and their role in PDN represents an important, yet understudied frontier in pain
105 and peripheral neuropathy research.

106 Using size exclusion chromatography, we obtained enriched keratinocyte-derived
107 exosomes from mice and performed an unbiased molecular cargo characterization with
108 proteomics and small RNA sequencing. We found that a high-fat diet-induced PDN mouse
109 model significantly altered the protein and microRNA content of keratinocyte-derived
110 exosomes compared to regular diet control mice. This included alterations in pathways
111 involved in axon guidance and synaptic transmission. Additionally, using an *in vivo*
112 conditional EV reporter mouse line, we demonstrated that epidermal-originating GFP-
113 tagged keratinocyte-derived exosomes are retrogradely trafficked into the DRG neuron
114 cell body. Overall, we present evidence that supports keratinocyte-derived exosomes as
115 a novel interaction pathway between epidermal keratinocytes and DRG neurons and that
116 altered cutaneous EV-trafficking may play a functional role in the development of the
117 small fiber neuropathy observed in PDN.
118

RESULTS

Keratinocytes release a diverse population of exosomes. To study keratinocyte-derived exosomes (KDEs), we cultured primary keratinocytes from adult mice as previously described[17,18]. After collecting cell-conditioned medium (CCM), we fractionated the CCM using a 35-nm pore size-exclusion chromatography column as previously described[43] (Figure 1A) and observed a corresponding increasing total protein concentration with each successive fraction (Figure 1B; silver stain). We immunoblotted for known exosome markers and found fractions 2 and 3 were enriched with the exosome-associated cargo markers Alix, Tsg101, and Syntenin-1 as well as the transmembrane tetraspanins CD63 and CD81[23-25,44] while being negative for GM130 and Calnexin, which are Golgi-associated proteins[45] (Figure 1B). Thus, pooled fractions 2 and 3, which represented our highly enriched KDE fractions with minimized free-floating protein contamination, were used for all subsequent analyses[46].

To investigate the role of KDEs in painful diabetic neuropathy, we employed the clinically relevant and well-established high-fat diet (HFD) model of PDN[47-50], where mice are fed either a regular diet (RD) or a diet with a high fat content for ten weeks, during which time they develop obesity, glucose intolerance and mechanical allodynia accompanied with small-fiber degeneration[48-50]. We cultured primary epidermal keratinocytes under the same conditions from RD or HFD mice. At 90% confluency, both RD and HFD cultures expressed keratin-14 (K14), a marker of undifferentiated, basal-layer keratinocytes, and keratin-10 (K10), a marker of differentiated keratinocytes (Supplemental Figure 1A). Additionally, cultured keratinocytes demonstrated a high degree of proliferative ability with Ki67 staining (Supplemental Figure 1B). Interestingly,

142 HFD keratinocytes maintained a phenotype of impaired wound healing after seven days
143 *in vitro* (Supplemental Figure 1C-D), consistent with findings in diabetic patients[51].
144 Fraction 2/3 KDEs were determined to have a size within the range of exosomes of 59.2
145 ± 14.5nm and 70 ± 26.3nm by dynamic light scattering and a concentration peak of 95 ±
146 6.1nm and 86 ± 8.7nm by nanoparticle tracking analysis for RD (Figure 1C-D) and HFD
147 (Supplemental Figure 2B-C), respectively, while TRPS determined that the mean size
148 average for RD KDEs were 97.7 ± 4.5nm with a concentration peak of 72.3 ± 4.5nm
149 (Figure 1E). KDEs from both RD and HFD were visualized via negative staining (Figure
150 1F) and cryo-electron microscopy (Figure 1G), which revealed the expected crescent
151 morphology and intact vesicular structure.

152 **Keratinocytes release soluble factors that encourage DRG neuron axonal growth.**
153 Given that the loss of cutaneous innervation is reported in PDN[13,14,49], we next sought to
154 investigate the role of KDEs on DRG axonal growth. We employed a microfluidics co-
155 culture system with primary adult mouse DRG neurons in one chamber and adult mouse
156 keratinocytes in the other (Figure 2A). This setup allowed for cell medium exchange only
157 through the microchannels between the chambers. Interestingly, we found that DRG
158 neuronal axons crossed the microchannels separating the two chambers at a higher rate
159 when grown in a co-culture with keratinocytes compared to when grown alone, indicating
160 that keratinocytes release soluble growth factors that promote axonal growth (Figure 2B-
161 C).

162 To test whether mouse KDEs are functional, we labeled them with DIR, which is a
163 lipophilic fluorescent dye that binds to lipid membranes, and applied them directly to
164 primary DRG neuron cultures. We observed a robust uptake of these KDEs by both the

165 cell bodies and neurites of the neurons (Figure 2D). To better model physiological
166 relevance, we then cultured DRG neurons in one chamber of our microfluidic system and
167 allowed their neurites to occupy all the microchannels, thus preventing the free flow of
168 medium between chambers. We then added DIR-labeled KDEs to the empty chamber to
169 test whether they could be transported through the neurites to the DRG neuron cell body.
170 Indeed, DIR-labeled KDEs were readily detected in the DRG neuron cell bodies 16 hours
171 post application, suggesting the retrograde transport of DIR-labeled KDEs through the
172 neurites[52] (Figure 2E). We next sought to investigate the cargo of these KDEs.

173 **Keratinocyte-derived exosomes alter their protein cargo in painful diabetic**
174 **neuropathy.** We characterized the KDE protein content in the context of PDN using a
175 proteomic approach[53]. The analysis was performed on the pooled fractions 2/3 using
176 liquid chromatography-tandem mass spectrometry (LC-MS/MS) for both RD and HFD
177 KDEs (Figure 3A). A gene ontology enrichment analysis on proteins detected in pooled
178 fractions 2/3 for both groups clustered in EV categories, suggesting a robust small EV
179 enrichment for both RD and HFD KDEs (Figure 3B). Importantly, we found similar
180 quantities based on the number of spectral counts of the canonical exosome-associated
181 proteins Alix, Tsg101, and Syntenin-1 in both samples (Figure 3C). Interestingly, fractions
182 2/3-enriched proteins also significantly clustered in the GO enrichment term 'Axon
183 Development,' (Figure 3C; Insert), suggesting a neuron-keratinocyte communication
184 pathway via exosomes. Moreover, we identified 128 differentially expressed exosome-
185 associated proteins (EAPs) between RD and HFD KDEs. There were 90 significant EAPs
186 with a fold change (FC) ≥ 1.5 with biological replicates clustering by group (Figure 3D-E).
187 Interestingly, one significant differentially expressed REACTOME pathway that arose was

188 the 'MAPK Family Signaling Cascades,' which included both Mapk1 and Mapk3 (Figure
189 3G left; Adjusted p-value ≤ 0.05), with Mapk1 validated in fraction 2/3 (Figure 3F).
190 Furthermore, a gene ontology enrichment analysis on the EAPs revealed 'Wound Healing'
191 (3G middle; Adjusted p-value ≤ 0.05), which is reported to be impaired in diabetic
192 patients[54] and persisted in our 2D primary HFD keratinocyte cultures (Supplemental
193 Figure 1C-D), as a significant differentially expressed pathway in the HFD KDEs. Notably,
194 several annexins arose, which are reported to play a role in ESCRT-III mediated plasma
195 membrane repair[55-58] and wound healing[55], with annexin VII confirmed in fraction 2/3 on
196 western blot (Figure 3F). As previously reported, DRG nerve afferents have been shown
197 to tunnel through the keratinocyte cytoplasm and form synapse-like contacts[20,21].
198 Interestingly, a differentially expressed pathway that arose was the GO term
199 'Neurotransmitter Secretion' (Figure 3G right; Adjusted p-value ≤ 0.05). These provide
200 compelling evidence of the neuron-keratinocyte communication pathway, which, at least
201 in our system, is altered in a HFD mouse model of PDN. We next sought to further
202 characterize the KDE cargo.

203 **The microRNA cargo of keratinocyte-derived exosomes is altered in painful**
204 **diabetic neuropathy.** Exosomes contain gene-modifying RNAs, with microRNAs being
205 the most abundant RNA species[43]. Several microRNAs have been associated with pain
206 in diabetic neuropathy[59], but the KDE microRNA content has not yet been identified in the
207 context of PDN. Hence, we next investigated the microRNA cargo of RD and HFD KDEs
208 using an unbiased small-library RNA sequencing approach.

209 Interestingly, we found that the top ten most abundant microRNAs identified,
210 including their variants, accounted for 74.8% of the total small RNA sequenced for both

211 groups (Figure 4A). Additionally, the top two hits, the let-7 and miR-23 families, accounted
212 for almost 40% of the total RNA sequenced for both groups. By cross-referencing 3
213 separate databases (Figure 2B), the predicted protein targets of these small RNAs were
214 used to run a KEGG enrichment analysis for let-7 and miR-23, with both revealing 'Axon
215 Guidance' as a predicted target pathway (Figure 4C). Between the RD and HFD KDEs,
216 there were 35 significant differentially expressed microRNAs that clustered by group
217 (Figure 4D) with 33 with a fold change (FC) ≥ 1.5 (Figure 4E). By cross-referencing the
218 same three databases, the predicted target proteins from each microRNA were run
219 through a gene ontology enrichment analysis with three producing significant target
220 pathways (Figure 4F; Supplemental Figure 3F-G). Both miR-684, which has been
221 implicated in multiple sclerosis[60], and miR24-3p, which has been studied in the context of
222 cancers[61,62] along with its regulation of proliferation related to annexin-6 activity[63],
223 revealed predicted target axon-guidance related pathways (Figure 4G), further providing
224 compelling evidence for a neuron-keratinocyte communication pathway via KDEs under
225 both normal physiology and PDN. Given both the proteomic and small RNA sequencing
226 datasets revealed predicted target pathways involved in axon guidance, and that painful
227 diabetic neuropathy is accompanied by peripheral nerve degeneration[49], we next
228 designed an *in vivo* animal model to investigate the interaction between KDEs and DRG
229 neuron afferent fibers.

230 **Epidermal keratinocyte-derived exosomes are fluorescently labeled with CD63-**
231 **emGFP**. We previously showed that, alongside the luminal exosome markers Alix,
232 Syntenin-1, and Tsg101, fraction 2/3 from our keratinocyte CCM consistently
233 immunoblotted for the transmembrane tetraspanins CD63 and CD81[24] (Figure 1B). We

234 employed the commercially available CD63-emGFP fl/fl mouse line (JacksonLaboratory
235 Strain#:036865) and crossed it with K14-Cre mice to generate a K14-CD63-emGFP EV
236 reporter mouse model (Figure 5A) to label exosomes originating from basal layer
237 keratinocytes and their progeny. We visualized a cross-section of skin with K14
238 immunohistochemistry staining and observed robust GFP expression throughout the
239 epidermis of these mice (Figure 5B), confirming basal layer keratinocytes and their
240 progeny express GFP in the epidermis only. Furthermore, we immunoblotted whole
241 epidermis cell lysate and detected both the membrane-bound CD63-GFP fusion protein
242 and soluble GFP (Figure 5C), presumably due to endogenous protein recycling. We next
243 cultured keratinocytes from this EV-reporter mouse. As expected, we observed a strong
244 GFP signal along the outer membrane of these keratinocytes (Figure 5D). We next
245 immunoblotted all ten fractions obtained from CCM of primary keratinocyte cultures for
246 GFP and detected a strong GFP signal, both the fusion and soluble forms, in fractions
247 2/3, which corresponded to our KDE enriched fractions (Figure 5E). Furthermore, isolated
248 GFP-labeled KDEs were functionally internalized by DRG neurons with GFP detected in
249 both the neuron cell bodies and neurites (Supplemental Figure 4A). Given the gene
250 ontology enrichment pathways highlighted from our proteomic and small RNA sequencing
251 experiments, we next sought to better understand the neuron-keratinocyte
252 communication pathway using our EV reporter mouse line.

253 **Epidermal keratinocyte-derived exosomes are retrogradely transported to the DRG**
254 **neuron cell bodies in male and female mice**. We further investigated the *in vivo*
255 conditional EV-reporter mouse, shifting our focus towards the DRGs. Notably, we
256 detected a GFP signal in DRG cross-sections from both RD and HFD EV-reporter mice

257 (Figure 6A; Supplemental Figure 4B) and not in WT DRG controls (Figure 6B).
258 Additionally, the cell lysate of K14-CD63-GFP (KCG) DRG neurons immunoblotted for
259 GFP (Figure 6C), further supporting the evidence for the retrograde transport of GFP-
260 positive epidermal exosomes to the DRG neuron cell bodies. We next cultured primary
261 DRG neurons from the EV-reporter mouse model for both RD and HFD. We observed
262 robust GFP expression in both groups (Figure 6D) with no GFP signal in WT controls
263 (Figure 6E). Interestingly, the GFP observed in these primary DRG neuron cultures
264 presented in the same pattern observed in the DIR-labeled exosomes (Figure 2D) and
265 GFP-labeled exosomes (Supplemental Figure 4A) applied to primary DRG cultures,
266 specifically as puncta[46]. Indeed, we detected these puncta in both the neuron cell bodies
267 and along the neurites (Figure 6F). These data strongly suggest that CD63-GFP-positive
268 keratinocyte-derived exosomes are retrogradely transported from the epidermis to DRG
269 neuron cell bodies, representing a novel mode of communication.

DISCUSSION

We isolated and characterized keratinocyte-derived exosomes (KDEs) morphologically and molecularly using an unbiased proteomic and small RNA sequencing approach. Our research revealed that KDEs alter their cargo in a mouse model of painful diabetic neuropathy (PDN), and we identified several gene ontology enrichment pathways that were significantly differentially expressed. In both “omic” datasets, neuron-keratinocyte pathways arose as significantly enriched both under normal physiology and in PDN. Additionally, we created a K14-CD63-emGFP extracellular vesicle (EV)-reporter mouse line and observed a GFP signal in the DRG neurons and neurites, suggesting keratinocyte-derived GFP-tagged exosomes are retrogradely trafficked from epidermal keratinocytes into the DRG neurons of mice.

These findings suggest a direct communication pathway between the epidermis and the peripheral nervous system, and that this is altered in our HFD mouse model of PDN. In our microfluidic paradigm, the presence of keratinocytes enhanced neurite outgrowth, indicating they release a soluble factor that encourages this growth (Figure 2A-C). Interestingly, proteomic analysis of our KDEs revealed that they contained several catenin and plexin isoforms (3C; Insert). The canonical WNT-signaling pathway plays a significant role in axon development in the central[64,65] and peripheral[66] nervous systems and has been implicated in Schwann cell-axon communication[67]. Plexins, the surface receptors for semaphorins, are involved in neuron axonal growth and guidance as well as a host of other functions[68-71]. Semaphorin 4C-Plexin-b2 signaling has been reported to be markedly increased in states of persistent pain in mice, and downregulation of this pathway led to the impairment of inflammatory hypersensitivity via the RhoA-ROCK-

293 dependent mechanisms[72]. Additionally, Sema3A and Plexin A were reported to be
294 dysregulated in the spinal cord of a HFD model of PDN[73]. To our knowledge, this is the
295 first report of these proteins being present as KDE cargo. Additionally, notch1, which was
296 recently reported to facilitate neuron-to-neuron communication through EVs in the
297 hippocampus of mice[46], was detected in our KDEs for all three biological replicates of
298 both diet groups (3C; Insert), suggesting this mechanism of internalization may also apply
299 to keratinocyte-neuron terminal endings in the skin. Notch-signaling is known to play a
300 prominent role in developing neurons, including in axon guidance[74,75]. Mutations in the
301 Notch-ligand Jagged1 was implicated in the development of peripheral neuropathy in two
302 independent families and confirmed in a mouse model[76]. Thus, Notch-signaling may
303 represent an unexplored, novel communication pathway between keratinocytes and DRG
304 neuron terminal nerve endings.

305 The KDEs from both groups contain differentially expressed synaptotagmin, which
306 is an essential component of the presynaptic vesicle release complex that facilitates
307 vesicle fusion with the plasma membrane[77,78], along with synaptophysin and synapsin-2,
308 both of which are involved in regulating vesicle docking to the inner plasma membrane[79-
309 81] (3G; Right Panel). These proteins have all been previously reported in keratinocytes[82].
310 However, it is still unclear why these proteins are present as KDE cargo and what their
311 function in keratinocyte-to-neuron communication might be. Further experiments are
312 required to validate all these cargo proteins, both in mice and human KDEs, and to
313 investigate their mechanism of action on nerve terminals.

314 Our small RNA sequencing dataset aligned with the proteomic data. The top two
315 most abundant small RNAs, let-7 and miR-23 (Figure 4A), were predicted to target

316 several prominent signaling pathways that overlapped with the proteomic dataset,
317 including MAPK signaling and the WNT signaling pathways (Figure 4C). A recent study
318 has indicated that partially inhibiting p38-MAPK activation in a diabetic neuropathy rat
319 model led to anti-hyperalgesic effects, suggesting a significant role for MAPKs in
320 nociception modulation[83]. KDEs from both our groups contained a diverse range of MAP-
321 kinases (MAPKs), with mapk1 differentially expressed in our HFD model. Both let-7 and
322 miR-23 have been shown to modulate MAPK activity[84,85]. Additionally, two differentially
323 expressed microRNAs suggested altered keratinocyte-to-neuron communication (Figure
324 4F-G). An altered expression of miR-24-3p has been reported in cancer[61,62,86,87] and
325 diabetes[88]. By cross-referencing three separate databases for predicted targets and
326 running a gene ontology enrichment analysis, one predicted pathway for miR-24-3p
327 modulation is plexin-semaphorin activity, and our proteomic dataset suggested plexin-b2
328 as a cargo protein (Figure 3C). However, the precise mechanism by which these
329 microRNAs regulate axon guidance and how they potentially contribute to PDN remain
330 unclear. Further studies are necessary to understand how these microRNAs modulate
331 target proteins and pathways, either directly or indirectly.

332 The DRG transcriptome is substantially altered in PDN[89] resulting in
333 hyperexcitability of the nociceptive neurons that drive neuropathic pain[49,89], presenting a
334 possible druggable system for future therapeutics. In our studies, using an EV-reporter
335 mouse line in which KDEs are labelled with CD63-emGFP (Figure 6A), we detected a
336 GFP signal in the DRG neuron cell bodies and neurites (Figure 6F). This indicates that
337 GFP-containing exosomes originating in the epidermis are retrogradely trafficked into the
338 DRG neuron cell body, where they can, presumably, initiate transcriptional changes due

339 to their cargo. It should be noted that the GFP species detected, at least from our
340 immunoblotting, was the non-fused form of GFP rather than the CD63-GFP fusion form
341 (Figure 6C), but that the soluble GFP was also detected in the epidermis (Figure 5C) and
342 KDE fractions (Figure 5E) in high abundance. It may be that the GFP-tagged exosomes
343 are trafficked to the DRG neurons, where they release their transcription-altering cargo,
344 and subsequently the fusion protein is then degraded into the soluble GFP that we
345 detected in immunoblotting.

346 This study enhances our understanding of the communication between
347 keratinocytes and DRG neurons and reveals a new role for KDEs in possibly promoting
348 axonal degeneration, which underlies neuropathic pain in PDN. As many genes show
349 differential expression in DRG neurons in PDN mice compared to control mice[90], our
350 studies support a novel strategy for treating PDN by focusing on the skin rather than the
351 entire body. One of the challenges with current PDN treatments is their systemic
352 administration and off-target effects[10-12]. Here, we present evidence for a delivery
353 pathway from epidermal keratinocytes to the peripheral nervous system, which could be
354 utilized to develop and deliver improved topical treatments for PDN and other nervous
355 system diseases. Additionally, our investigation into the role of exosome-mediated
356 communication between keratinocytes and DRG neurons has broader implications.
357 Indeed, exosomes hold great promise as novel disease biomarkers, therapeutic agents,
358 and drug delivery systems. This potential extends beyond PDN, laying the groundwork
359 for exploring new avenues in pain and peripheral neuropathy research and treatment.

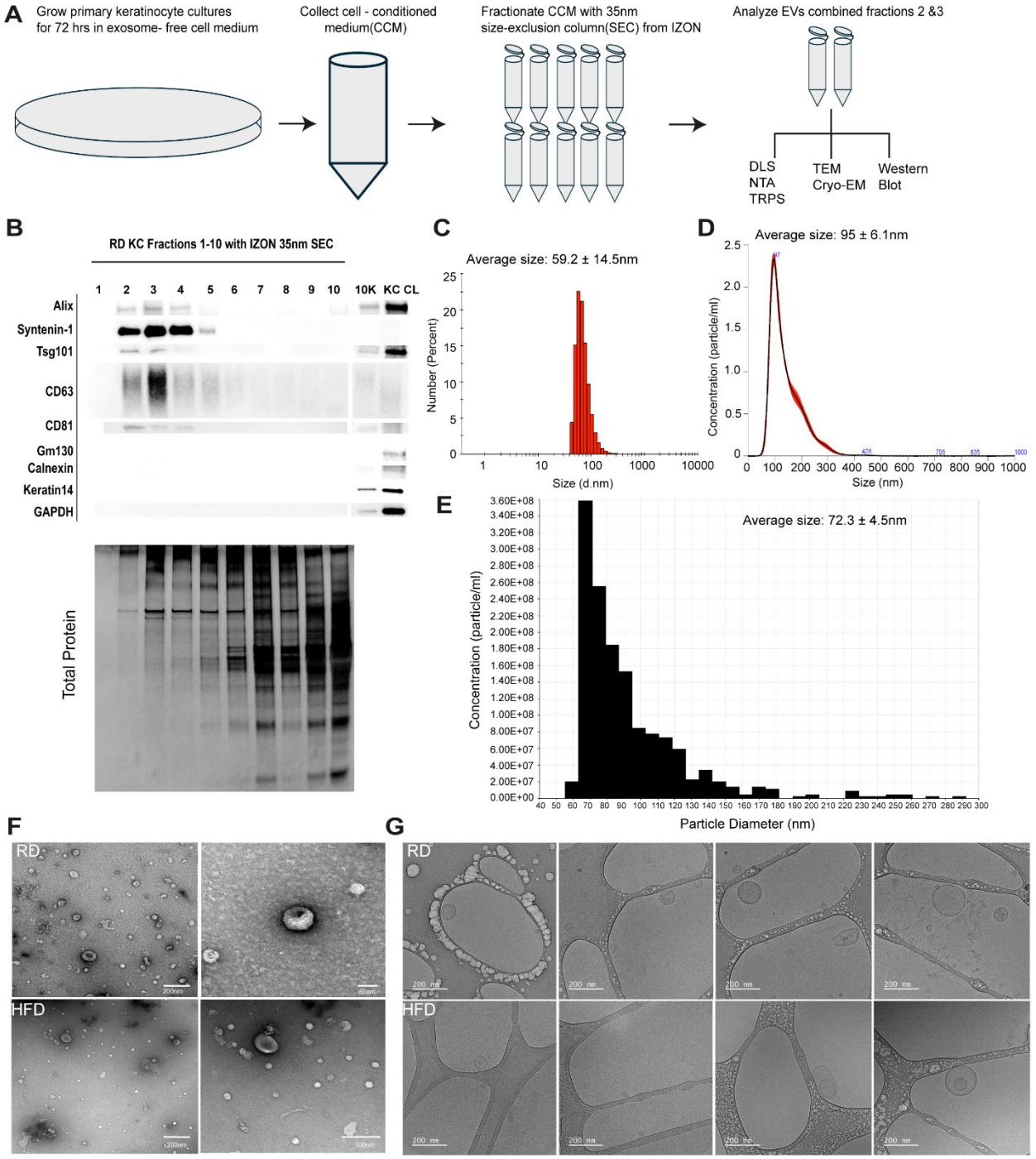

Figure 1: Keratinocytes release a diverse population of exosomes. A) Workflow schematic for keratinocyte-derived exosome (KDE) isolation using size exclusion chromatography (SEC). **B)** Immunoblotting the ten SEC fractions revealed exosome-associated proteins ALIX, Syntenin, Tsg101, CD63 and CD81 were enriched in fractions

364 2 and 3 relative to the total protein concentration (silver stain). **C)** KDEs analyzed with
365 dynamic light scattering had a size range of 59.2 ± 14.5nm (mean ± StDev). N=7
366 across biological replicates from both male and female mice. **D)** KDEs analyzed using
367 nanoparticle tracking analysis produced a concentration peak particle size of 95 ± 6.1
368 nm (mean ± StDev). N=2 male biological replicates. **E)** KDEs analyzed using tunable
369 resistive pulse sensing (TRPS) determined that the mean size average for RD KDEs
370 were 97.7 ± 4.5nm with a concentration peak of 72.3 ± 4.5nm (mean ± StDev). N=3
371 different pressures for one male. **F)** Nanovesicles from combined fraction 2/3 were
372 visualized with negative stain EM. N=11 across 5 biological replicates from male and
373 female mice. **G)** Combined SEC fractions 2/3 were visualized with cryo-EM,
374 demonstrating several diverse populations. N=2 biological replicates, one male and one
375 female.

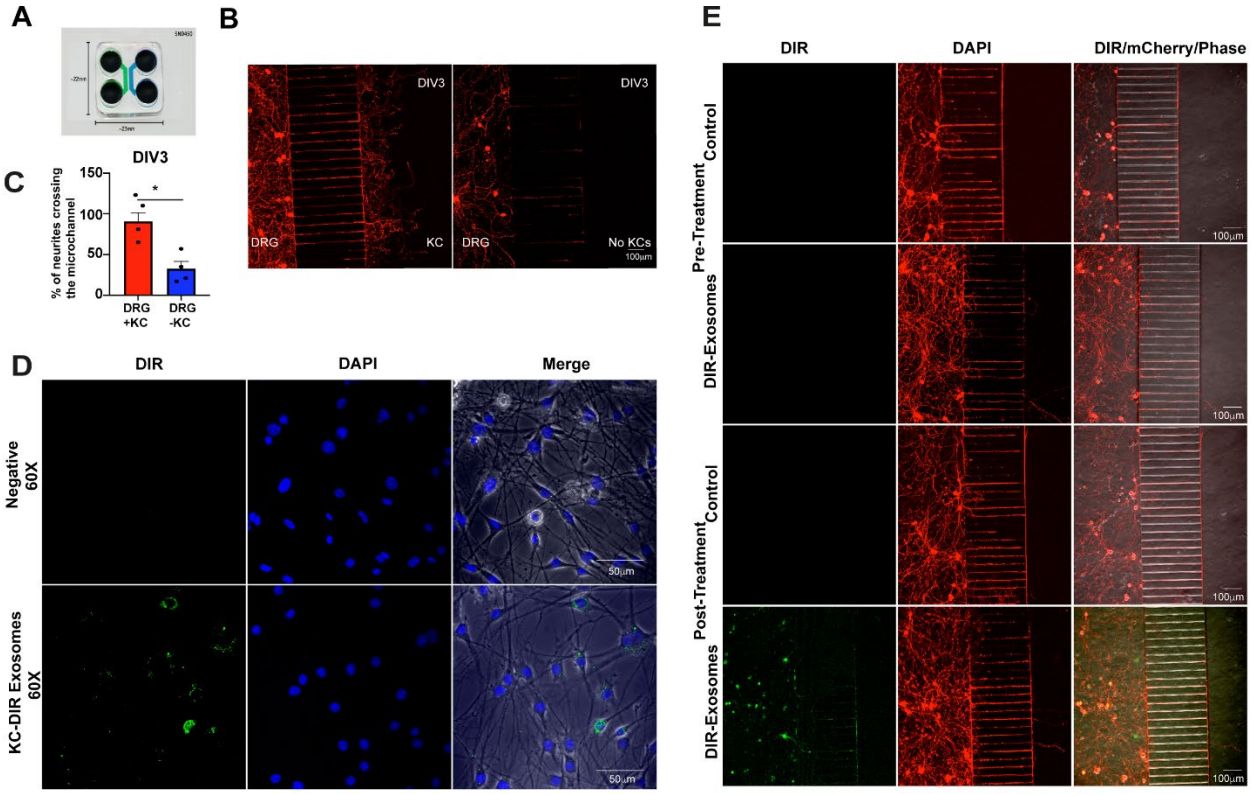

Figure 2: Isolated exosomes from SEC fraction 2/3 are functionally retrogradely trafficked by DRG neurons *in vitro*. A) Representative picture of microfluidics device. **B)** The presence of keratinocytes co-cultured with DRG neurons in a microfluidic paradigm encouraged neurite outgrowth crossing through the microchannels connecting both chambers. **C)** We observed a significant increase in the neurite microchannel crossing when co-cultured in the presence of keratinocytes ($p \leq 0.05$, one-tailed, paired t-test; n=5 with KCs and n=4 without KCs paired with DRG primary cultures). **D)** KDEs from SEC Fr2/3 are functionally internalized by primary DRG neurons. N=4 across 2 biological replicates. **E)** KDEs are retrogradely trafficked into the neuron cell body through the neurites in a microfluidic paradigm. N=4 biological replicates.

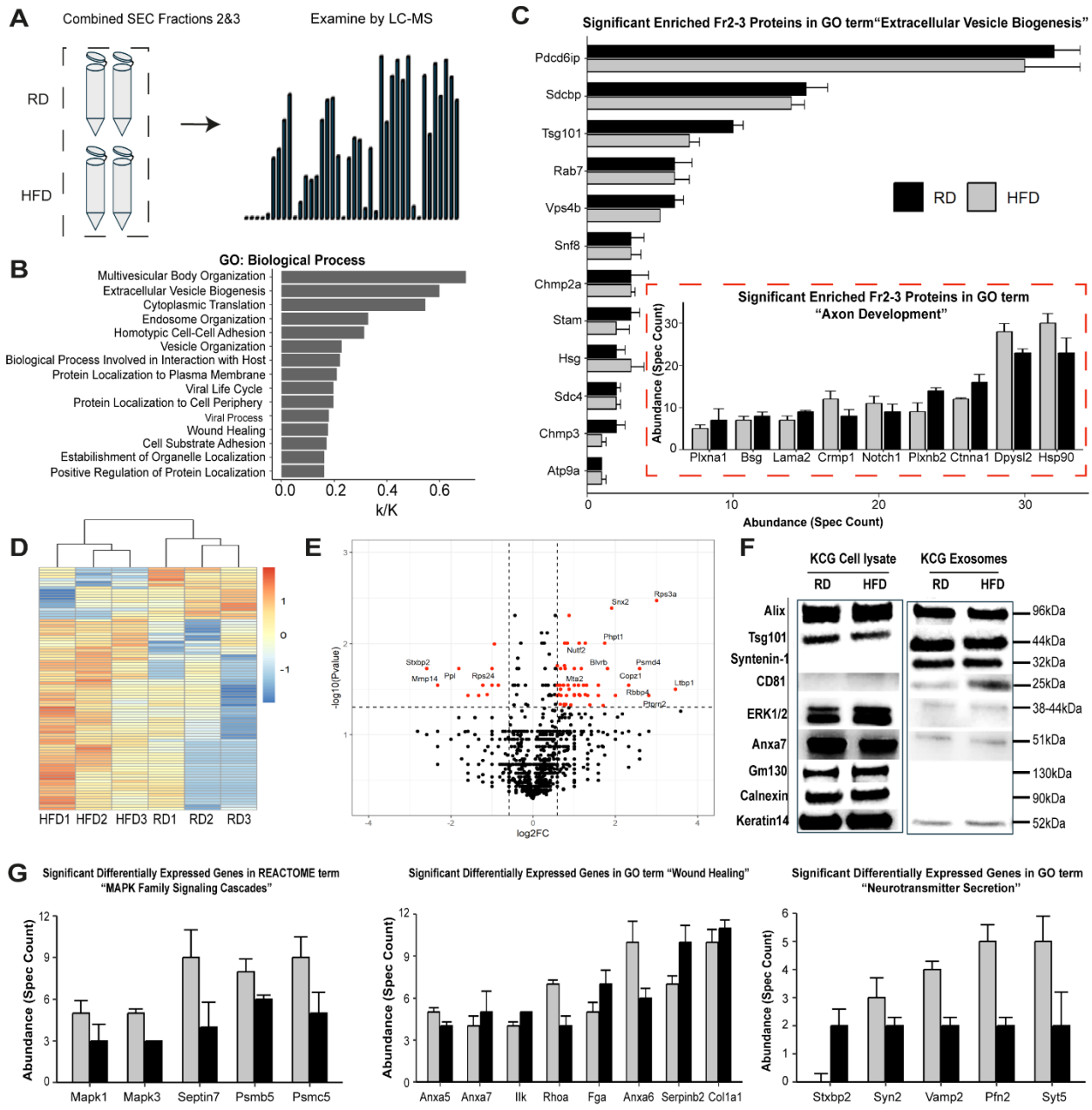

Figure 3: Keratinocyte-derived exosomes (KDEs) significantly alter their protein cargo in painful diabetic neuropathy. A) Workflow schematic depicting exosome proteomic analysis. N=3 biological replicates for each group from male mice. **B)** The top pathways from a gene ontology enrichment analysis of proteins present in each of the three biological replicates in both experimental groups suggested EV enrichment.

391 Bonferroni adjusted p-value ≤ 0.01. **C)** Select panel of proteins associated with GO Term
392 'EV Biogenesis' revealed similar spectral counts for exosome markers Alix, Syntenin-1,
393 and Tsg101 between both groups. Insert: GO Term 'Axon Development' revealed several
394 unverified notable proteins as exosome cargo. Mean ± SEM. GO Terms Bonferroni
395 adjusted p-value ≤ 0.01. **D)** There were 128 significant differentially expressed exosome-
396 associated proteins (EAPs) (paired t-test, one-way, p≤0.05) between RD and HFD KDEs.
397 We observed 90 significant EAPs with a ≥ 1.5-fold change (FC) that clustered by group.
398 FC calculated as average HFD/RD spectral count for each protein. **E)** Representative
399 volcano plot with the 128 EAPs. EAPs with an FC ≥ 1.5 are labelled red. **F)** Western blot
400 confirms two EAPs, Mapk1 (via ERK1/2 expression) and annexin-7 in SEC Fr2/3. n=3
401 biological replicates for each group. **G)** Abundances for EAPS in the differentially
402 expressed GO term 'Wound Healing,' 'Neurotransmitter Secretion,' and the REACTOME
403 term 'MAPK Family Signaling Cascades.' Mean ± SEM. Bonferroni adjusted p-value ≤
404 0.01.

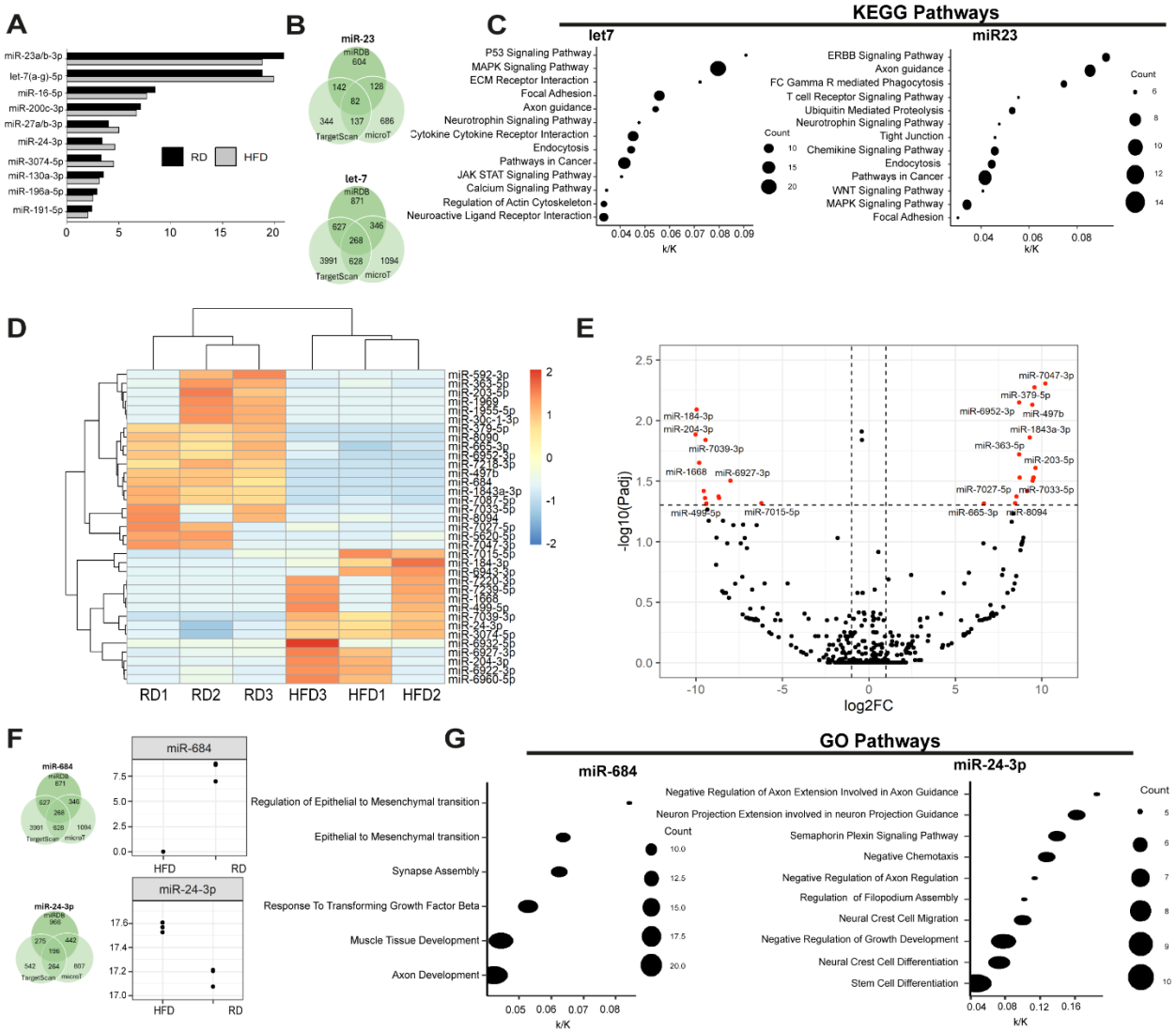

Figure 4: Keratinocyte-derived exosomes (KDEs) alter their small RNA cargo in painful diabetic neuropathy. N=3 biological replicates for male mice in each diet group. A) The top ten small RNAs identified in both RD and HFD KDEs represent 74.8% of the total small RNA sequenced. The top two small RNAs, the let-7 and microRNA-23 families, accounted for almost 40% of the total small RNA sequenced. **B)** The predicted protein targets for let-7 and miR-23 were obtained by cross-referencing 3 separate databases: MirDB, TargetScan, and DIANA-microT. The protein targets predicted by all three programs were used for downstream analysis. **C)** The enrichment analysis of the

413 predicted protein targets of let-7 and miR-23 both revealed predicted KEGG pathways
414 related to 'Axon Guidance,' suggesting a possible role of KDE small RNAs on
415 keratinocyte-to-neuron communication. KEGG pathways Bonferroni adjusted p-value ≤
416 0.01. **D)** There were 35 differentially expressed microRNAs, which clustered by group.
417 Bonferroni adjusted p-value ≤ 0.05. **E)** Of the 35 differentially expressed microRNAs, 33
418 had a fold change ≥ 1.5 between RD and HFD, with 22 overexpressed in HFD. FC is
419 defined as HFDavg/RDavg microRNA counts for each small RNA. Bonferroni adjusted p-
420 value. **F)** miR-684 was downregulated in HFD while miR-24-3p was upregulated. Using
421 the same three databases as Figure 4B, predicted target proteins lists were obtained for
422 each. **G)** The gene ontology enrichment analysis for these predicted proteins presented
423 several interesting GO Terms. Both differentially expressed microRNAs predicted axon-
424 related pathways, further providing evidence for an altered keratinocyte-to-neuron
425 communication via exosome cargo. GO Terms Bonferroni adjusted p-value ≤ 0.01.

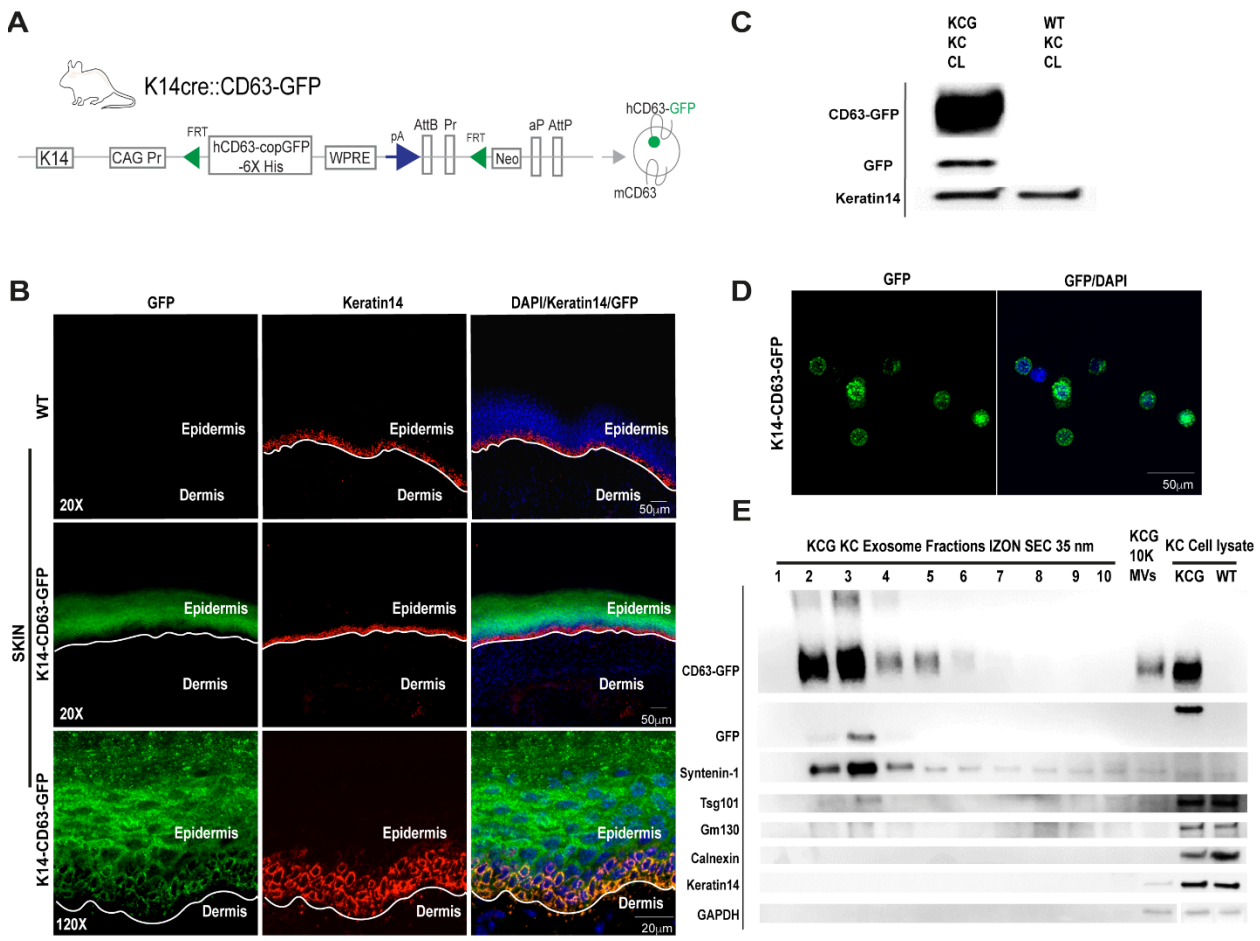

Figure 5: Epidermal keratinocyte-derived exosomes (KDEs) are enriched with GFP in an EV-reporter mouse model. A) We created an EV-reporter mouse line by crossing the commercially available CD63-GFP fl/fl mouse line with K14-Cre to create K14-CD63-GFP (KCG) mice. **B)** IHC on cryo-sections of glabrous mouse skin demonstrated GFP expression in all layers of the epidermis with no detectable GFP in the dermis. The GFP signal also co-localized with K14 staining, representing the basal layer of the epidermis. **C)** Immunoblotting revealed robust GFP signal in epidermal cell lysate from our EV-reporter mouse line. **D)** GFP was detected in the primary keratinocyte cultures from our EV-reporter mouse line. **E)** Cell-conditioned medium from KCG keratinocyte cultures was run through IZON 35nm SEC columns. Fraction 2/3 was enriched with CD63-GFP and

436 soluble GFP, supporting that KDEs from primary cultured keratinocytes from our EV-
437 reporter mouse line are tagged with the CD63-GFP fusion protein.

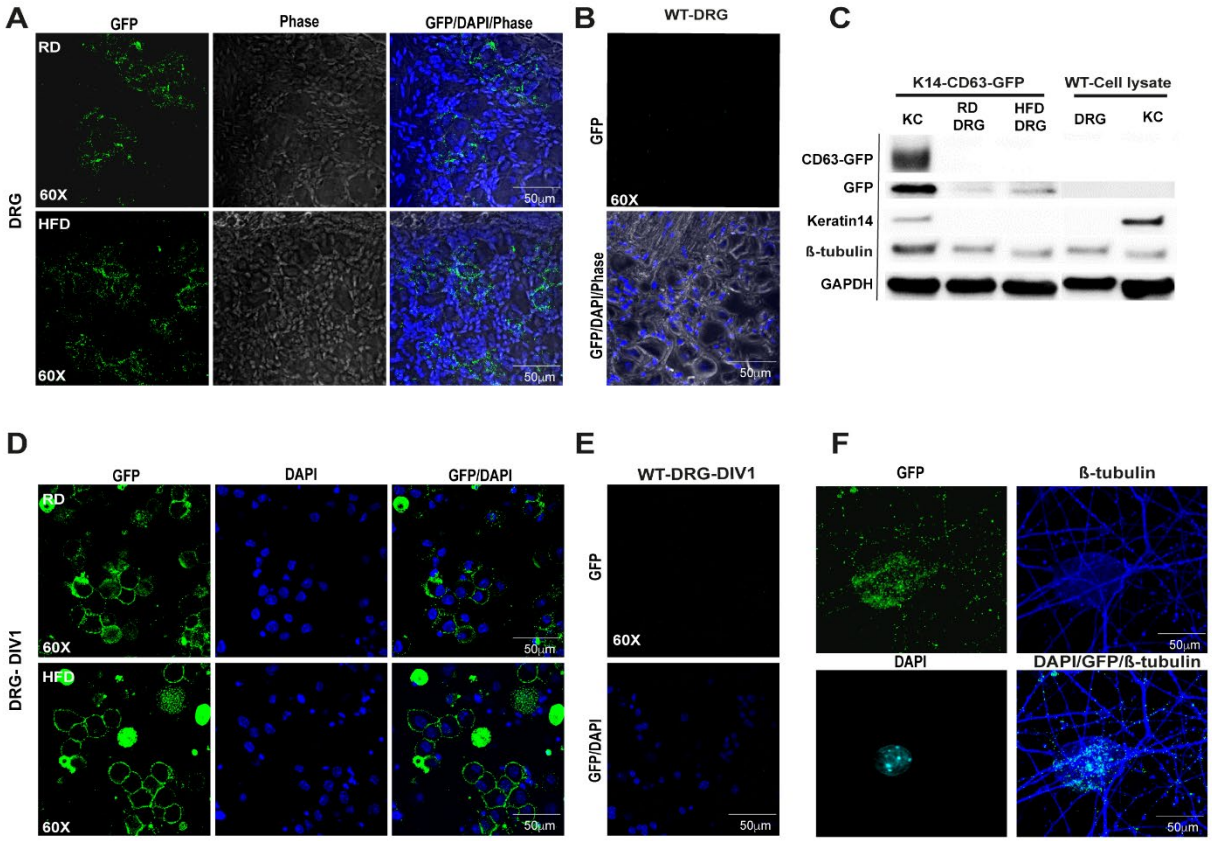

Figure 6: Epidermal keratinocyte-derived exosomes (KDEs) are retrogradely trafficked from the epidermis to DRG neurons *in vivo* in male and female mice. A) We detected GFP signal after immunolabeling amplification in cryosections of the DRGs from the EV-reporter mice for both RD and HFD. N=3 male biological replicates for both RD and HFD and n=2 for RD female mice. **B)** As expected, no false GFP signal was detect in WT DRG cryosections. N=3 biological replicates of WT. **C)** Immunoblotting the DRG cell lysate of EV-reporter mice revealed GFP expression. N=2 biological replicates for both RD and HFD. **D)** We detected GFP signal after IHC amplification in primary DRG cell cultures from the EV-reporter mice for both RD and HFD. N=3 biological replicates for both RD and HFD. **E)** As expected, no false GFP signal was detected in WT primary DRG cultures. N=3 biological replicates of WT. **F)** The GFP signal was not only detected

449 in the cell body of the primary DRG cultures from EV-reporter mice but also along the
450 neurites, further providing evidence that KDEs are trafficked along the neurites. N=6
451 biological replicates between RD and HFD.

452 **METHODS**

453 ***Animals*.** Animals were housed on a 12-hour light/12-hour dark cycle with ad libitum
454 access to food and water. We used the following mouse lines: K14-Cre, homozygous;
455 CD63-emGFP fl, homozygous; K14-Cre::CD63-emGFP fl heterogenous.

456 ***HFD*.** Mice were fed 42% fat (Envigo TD88137) for 10 weeks as a rodent model of type 2
457 diabetes. Control mice were fed a regular diet (RD) of 11% fat. After 10 weeks of RD or
458 HFD, a glucose tolerance test was performed as described[49]. A cutoff of (≥140 mg/dl) at
459 2 SD above the mean for glucose 120 minutes after glucose challenge in WT littermate
460 mice was used as a 'diabetic' classification[49].

461 ***Behavioral testing*.** von Frey behavioral studies were performed as previously
462 described[49] with random experimental group assignments and double-blind investigator
463 and endpoint analysis conditions.

464 ***Primary keratinocyte cultures*.** Glabrous paw skin is dissected from the mouse and
465 incubated in dispase (2.3 mg/ml) overnight. The epidermis is separated from the dermis
466 and incubated in TrypLE Express (10 min, 37C; Gibco 12604-013); the keratinocytes are
467 dislodged using gentle agitation with forceps and then plated on 15cm^2 plates with 154CF
468 epidermal medium (M154CF500) supplemented with 170ul of 0.2M $CaCl_2$ and 5ml of
469 HKGS (S-001-5), which was depleted of EVs following 18 hours of ultracentrifugation at
470 100,000*g*. Medium change occurs 24 hours after plating and then every 48 hours.
471 Complete cell culture medium and all other reagents have been confirmed to be EV-free
472 prior to use with the keratinocyte cultures.

473 ***Wound healing scratch assay*.** Primary keratinocyte cultures were grown on 6-well
474 plates (Fisherbrand FB012927) with a 300,000-seeding density and grown to 90%

475 confluency. The tip of an Eppendorf 200ul pipette tip (Fisher 02707409) was used to form
476 a vertical scratch down the center. Cultures were tracked every 24 hours on a Leica 2000
477 LED microscope and analyzed using ImageJ software to measure the rate of gap closure.
478 One-tail paired t-tests were used on the raw dataset to obtain a p-value between groups
479 for each time point (n=58 RD, n=61 HFD for each time point across three separate
480 biological replicates for each group; significance $p \leq 0.05$).

481 ***Exosome isolation with size exclusion columns.*** Cell-conditioned medium from
482 keratinocyte cultures is collected between culture confluency of 60-90%, is centrifuged at
483 3000*g* for 30 minutes to remove cell debris and is then concentrated to 500 µl using
484 centrifuge size filters (Pierce Protein Concentrators PES 10K, 88528). The sample is then
485 run through an IZON SEC qEV 35nm column (IZON, ICO-35) as previously reported[43].
486 Fractions 2-3 are used for downstream applications.

487 ***Western Blot.*** Fractions 1-10 of 400ul each are concentrated to 20ul using Millipore
488 centrifuge filters (Microcon 30kDa, MRCF0R030) and combined with one volume
489 equivalent of BioRad 2x Lammalenni loading buffer (BioRad 1610737) with 5% BME.
490 Each fraction is run through a 3-15% gradient gel (BioRad 45610840) alongside full
491 keratinocyte cell lysate (+) and a 10K pellet (large EVs), running a BCA assay (Thermo
492 Scientific) to load ~3 µg of protein per well. Protein was then transferred to PVDF
493 membranes (Millipore) and blocked (BioRad Everyblot 12010020) for 15 minutes. Primary
494 antibodies are applied overnight at 4 °C with secondary antibody at room temperature for
495 2 hours with 3 TBST washes between each step. Proteins are visualized with a
496 chemiluminescence detection system (Thermo Scientific 32209). All western blot gels
497 were run at minimum in triplicate. Blots were visualized on a Li-Cor Odyssey Fc.

498 ***Western blot antibodies.*** The following primary antibodies were used: Alix (Abcam
499 ab88388), Syntenin-1 (Abcam ab19903), Tsg101 (Invitrogen PA531260), CD63
500 (Invitrogen 2H5I1), CD81 (Abcam ab109201), GM130 (Abcam ab52649), Calnexin
501 (Abcam ab22595), K14 (BioLegend 906004), GFP (Abcam ab13970), β-tubulin
502 (ProteinTech 80713-1-RR100UL), GAPDH (Abcam ab181602). The following secondary
503 antibodies were used: Goat anti-rabbit HRP (Abcam ab97080), Goat anti-chicken HRP
504 (Invitrogen A16054).

505 ***Dynamic light scattering.*** 80ul of samples are pipetted into cuvettes (Malvern
506 Catalog#759200) and run through the zetasizer spectrophotometer (Malvern Zetasizer
507 Nano ZSP) with an EV refractive index of 1.35 in ANTEC through Northwestern University.
508 Malvern analytical software is used to analyze the output using particle counts relative to
509 the signal intensity.

510 ***Negative stain EM.*** Samples suspended in PBS are prepared using the standard uranyl
511 acetate fixation for 5 mins seeded on EMS grids (TMS Catalog#71150) and imaged on a
512 FEI Spirit 2 electron microscope. Images were processed using ImageJ software.

513 ***Cryo-EM.*** CryoEM images are obtained through the northwestern BioCryo core facility
514 (NUANCE) with samples prepared as previously described[91].

515 ***Primary DRG Cultures.*** DRG sensory neurons from WT and K14-CD63-GFP mice were
516 dissociated as described[92] at 18 weeks of age.

517 ***Microfluidics.*** Primary DRG cultures were deposited into one compartment chamber
518 connected to the microchannel column in a microfluidic system (XONA Microfluidics
519 SND450) with or without primary keratinocyte cultures in the other compartment
520 chambers. Keratinocytes were cultured for 3 days before depositing DRG cultures unless

521 otherwise specified. The medium was a combination of 50% DRG culture medium as
522 previously described[92] and 50% keratinocyte culture medium when both cell types were
523 present in the chambers.

524 ***DIR Labelling.*** Concentrated CCM was labeled with DIR (Invitrogen D12731; 2ug/ul) at
525 a ratio of 1:100 by volume and then passed through the IZON 35nm columns. Isolated
526 DIR-labeled exosomes from fractions 2-3 were then used for downstream applications
527 with a negative DIR control, which was DIR-added to concentrated EV-depleted
528 unconditioned medium passed through the column with the same fractions collected for
529 experiments.

530 ***DIR-Exosomes***. DRG Cultures: DIR-labeled exosomes were directly applied to DIV-1
531 primary DRG cultures and visualized after 16 hours post-treatment by confocal
532 microscopy. Microfluidics: DIR-exosomes were applied to the empty compartment after
533 DRG neuron neurites occupied all microchannels, preventing medium exchange between
534 the two compartments. The microfluidic chambers were visualized after 16 hours by
535 confocal microscopy.

536 ***MS sample preparation***

537 Trichloroacetic acid (TCA, Sigma-Aldrich, Cat# T0699) precipitation was used to clean
538 and precipitate proteins from EV samples. Protein pellets were resuspended in 8 M urea
539 (ThermoFisher Scientific, Cat # 29700) prepared in 100 mM ammonium bicarbonate
540 solution (Fluka, Cat # 09830) and processed with ProteaseMAX (Promega, Cat # V2072)
541 according to the manufacturer's protocol. The samples were reduced with 5 mM Tris(2-
542 carboxyethyl)phosphine (TCEP, Sigma-Aldrich, Cat # C4706; vortexed for 1 hour at RT),
543 alkylated in the dark with 10 mM iodoacetamide (IAA, Sigma-Aldrich, Cat # I1149; 20 min

544 at RT), diluted with 100 mM ABC, and quenched with 25 mM TCEP. Samples were diluted
545 with 100 mM ammonium bicarbonate solution, and digested with Trypsin (1:50, Promega,
546 Cat # V5280) for overnight incubation at 37°C with intensive agitation. The next day,
547 reaction was quenched by adding 1% trifluoroacetic acid (TFA, Fisher Scientific, O4902-
548 100). The samples were desalted using Peptide Desalting Spin Columns (Thermo Fisher
549 Scientific, Cat # 89882). All samples were vacuum centrifuged to dry.

550 ***Tandem Mass spectrometry***

551 Three micrograms of each sample were auto-sampler loaded with a Thermo Vanquish
552 Neo UHPLC system onto a PepMap™ Neo Trap Cartridge (Thermo Fisher Scientific,
553 Cat#: 174500, diameter, 300 µm, length, 5 mm, particle size, 5 □m, pore size, 100 Å,
554 stationary phase, C18) coupled to a nanoViper analytical column (Thermo Fisher
555 Scientific, Cat#: 164570, diameter, 0.075 mm, length, 500 mm, particle size, 3 µm, pore
556 size, 100 Å, stationary phase, C18) with stainless steel emitter tip assembled on the
557 Nanospray Flex Ion Source with a spray voltage of 2000 V. An Orbitrap Ascend (Thermo
558 Fisher Scientific) was used to acquire all the MS spectral data. Buffer A contained 99.9%
559 H2O and 0.1% FA, and buffer B contained 80.0% ACN, 19.9% H2O with 0.1% FA. For
560 each fraction, the chromatographic run was for 2 hours in total with the following profile:
561 0-8% for 6, 8% for 64, 24% for 20, 36% for 10, 55% for 10, 95% for 10 and again 95% for
562 6 We used Orbitrap HCD-MS2 method for these experiments. Briefly, ion transfer tube
563 temp = 275 °C, Easy-IC internal mass calibration, default charge state = 2 and cycle time
564 = 3 s. Detector type set to Orbitrap, with 60K resolution, with wide quad isolation, mass
565 range = normal, scan range = 375-1500 m/z, max injection time mode = Auto, AGC target
566 = Standard, microscans = 1, S-lens RF level = 60, without source fragmentation, and

567 datatype = Profile. MIPS was set as on, included charge states = 2-7 (reject unassigned).
568 Dynamic exclusion enabled with n = 1 for 60s exclusion duration at 10 ppm for high and
569 low with Exclude Isotopes. Isolation Mode = Quadrupole, isolation window = 1.6, isolation
570 Offset = Off, active type = HCD, collision energy mode = Fixed, HCD collision energy type
571 = Normalized, HCD collision energy = 25%, detector type = Orbitrap, orbitrap resolution
572 = 15K, mass range = Normal, scan range mode = Auto, max injection time mode = Auto,
573 AGC target = Standard, Microscans = 1, data type = Centroid.mins receptively.

574 ***MS data analysis and quantification***

575 Protein identification/quantification and analysis were performed with Integrated
576 Proteomics Pipeline - IP2 (Bruker, Madison, WI. http://www.integratedproteomics.com/)
577 using ProLuCID[93,94], DTASelect2[95,96], Census and Quantitative Analysis. Spectrum raw
578 files were extracted into MS1, MS2 files using RawConverter
579 (http://fields.scripps.edu/downloads.php). The tandem mass spectra (raw files from the
580 same sample were searched together) were searched against UniProt mouse
581 (downloaded on 07-29-2023) protein databases[97] and matched to sequences using the
582 ProLuCID/SEQUEST algorithm (ProLuCID version 3.1) with 50 ppm peptide mass
583 tolerance for precursor ions and 600 ppm for fragment ions. The search space included
584 all fully and half-tryptic peptide candidates within the mass tolerance window with no-
585 miscleavage constraint, assembled, and filtered with DTASelect2 through IP2. To
586 estimate protein probabilities and false-discovery rates (FDR) accurately, we used a
587 target/decoy database containing the reversed sequences of all the proteins appended
588 to the target database[97] (UniProt, 2015). Each protein identified was required to have a
589 minimum of one peptide of minimal length of six amino acid residues. After the

590 peptide/spectrum matches were filtered, we estimated that the protein FDRs were ≤ 1%
591 for each sample analysis. Resulting protein lists include subset proteins to allow for
592 consideration of all possible protein isoforms implicated by at least three given peptides
593 identified from the complex protein mixtures. Then, we used Census and Quantitative
594 Analysis in IP2 for protein quantification. Static modification: 57.02146 C for
595 carbamidomethylation. Quantification was performed by the built-in module in IP2.

596 ***Proteomics Statistics.*** The spectral counts for each protein accession ID for the three
597 RD and HFD biological replicates are used to run a one-tailed, paired t-test for statistical
598 significance. The average spectral counts for RD and HFD were used to obtain a HFD/RD
599 fold change. The volcano plot was generated in R using ggplot2. The heat map was
600 generated using the R package pheatmap. Gene ontology enrichment analyses were
601 generated using the R packages clusterprofiler, msigdbr and ggplot2. GO enrichment
602 analyses used proteins present in all biological replicates of each group only.

603 ***Small RNA sequencing.*** Samples underwent small RNA sequencing through
604 Northwestern's core facilities. Biological triplicate RD and HFD RNA samples were
605 prepared using the total exosome RNA and protein extraction kit from Invitrogen
606 (Invitrogen Catalog#2743605). RNA samples were quantified by Qubit RNA HS assay
607 and the quality was confirmed by Bioanalyzer RNA pico chip assay. Then, 1ng of RNA
608 was used as input for library preparation with NextFlex small RNA-seq kit v4 according to
609 manufacturer's protocol. Each sample was barcoded with a unique index and multiplexed
610 libraries were pooled for sequencing on Novaseq X Plus 10B flowcell using single end
611 50nt mode.

612 ***RNA sequencing Statistics.*** Data analysis was carried out in R using the standard
613 workflow of DESeq2 paired with the libraries apeglm and ggplot2 for figure generation.
614 Bonferroni post-hoc adjustment was used for the reported adjusted p-values ≤ 0.05 for
615 significance. Gene ontology enrichment analyses were generated using the R packages
616 clusterprofiler, msigdbr and ggplot2 with Bonferroni post-hoc adjusted P values < 0.05 for
617 significance.

618 ***Protein target analysis.*** The direct or indirect protein targets for each microRNA was
619 predicted using several target prediction programs, including miRDB (http://mirdb.org/)[98],
620 TargetScan v7.0 (http://www.targetscan.org/vert_72/) and DIANA-microT v5.0
621 (https://bio.tools/DIANA-microT). Only the predicted proteins identified by all 3 programs
622 were included in the subsequent enrichment analyses.

623 ***Immunohistochemistry.*** Glabrous hind paw dermis/epidermis was separated from the
624 paw and whole DRGs (lumber 2-4) were isolated from 18 week old mice and fixed with
625 4% PFA for 1 hour, 30% sucrose for 1 hour, and then embedded in OCT. Samples were
626 processed as previously described[50] and analyzed by confocal microscopy.

627 ***Antibodies.*** We used the following primary antibodies on DRG sections: GFP (chicken;
628 Abcam ab13970). We used the following antibodies on skin sections: K14 (BioLegend
629 906004). We used the following antibodies on primary DRG cultures: GFP (Abcam
630 ab13970), β-tubulin (ProteinTech 80713-1-RR100UL). We used the following secondary
631 antibodies: Goat anti-chicken AlexaFluor™-598 (Invitrogen A-11042), goat anti-rabbit
632 AlexaFluor-647 (Invitrogen A32733).

633 ***EV-Reporter Mouse.*** The commercially available CD63-GFP fl/fl mouse line (Jackson
634 Laboratory Strain#:036865) was crossed with K14-Cre mice to generate the EV-reporter
635 K14-CD63-GFP mouse line.
636 ***Study approval.*** All methods involving animals were approved by the IACUC of
637 Northwestern University.
638

639 **ACKNOWLEDGEMENTS**

640 Zetasizer Nano ZSP (DLS), Nanosight (NTA), and IZON Exoid (TRPS) experiments were
641 performed in the Analytical bioNanoTechnology Equipment Core Facility of the Simpson
642 Querrey Institute for BioNanotechnology at Northwestern University. ANTEC receives
643 partial support from the Soft and Hybrid Nanotechnology Experimental (SHyNE)
644 Resource (NSF ECCS-2025633) and Feinberg School of Medicine, Northwestern
645 University. Electron microscopy imaging work was performed at the Northwestern
646 University Center for Advanced Microscopy (RRID: SCR_020996) generously supported
647 by NCI CCSG P30 CA060553 awarded to the Robert H Lurie Comprehensive Cancer
648 Center. This work made use of the EPIC facility of Northwestern University's
649 NUANCE Center, which has received support from the SHyNE Resource (NSF ECCS-
650 2025633), the IIN, and Northwestern's MRSEC program (NSF DMR-2308691). And this
651 work was supported by the Northwestern University NUSeq Core Facility.
652

653 **STATEMENT OF DATA AND MATERIALS**

654 We will make the raw MS data publicly available in an accessible database upon
655 acceptance.

656 ## REFERENCES

657 1 Martin, S. S. *et al.* 2024 Heart Disease and Stroke Statistics: A Report of US and Global Data From
658 the American Heart Association. *Circulation* **149**, e347-e913 (2024).
659 https://doi.org/10.1161/CIR.0000000000001209
660 2 American Diabetes, A. Diagnosis and classification of diabetes mellitus. *Diabetes care* **34 Suppl 1**,
661 S62-69 (2011). https://doi.org/10.2337/dc11-S062
662 3 Dyck, P. J. *et al.* The Rochester Diabetic Neuropathy Study: design, criteria for types of neuropathy,
663 selection bias, and reproducibility of neuropathic tests. *Neurology* **41**, 799-807 (1991).
664 4 Spallone, V., Lacerenza, M., Rossi, A., Sicuteri, R. & Marchettini, P. Painful diabetic polyneuropathy:
665 approach to diagnosis and management. *The Clinical journal of pain* **28**, 726-743 (2012).
666 https://doi.org/10.1097/AJP.0b013e318243075c
667 5 Abbott, C. A., Malik, R. A., van Ross, E. R., Kulkarni, J. & Boulton, A. J. Prevalence and characteristics
668 of painful diabetic neuropathy in a large community-based diabetic population in the U.K. *Diabetes*
669 *care* **34**, 2220-2224 (2011). https://doi.org/10.2337/dc11-1108
670 6 daCosta DiBonaventura, M., Cappelleri, J. C. & Joshi, A. V. A longitudinal assessment of painful
671 diabetic peripheral neuropathy on health status, productivity, and health care utilization and cost.
672 *Pain medicine* **12**, 118-126 (2011). https://doi.org/10.1111/j.1526-4637.2010.01012.x
673 7 Bril, V. *et al.* Evidence-based guideline: Treatment of painful diabetic neuropathy: report of the
674 American Academy of Neurology, the American Association of Neuromuscular and
675 Electrodiagnostic Medicine, and the American Academy of Physical Medicine and Rehabilitation.
676 *Neurology* **76**, 1758-1765 (2011). https://doi.org/10.1212/WNL.0b013e3182166ebe
677 8 Quilici, S. *et al.* Meta-analysis of duloxetine vs. pregabalin and gabapentin in the treatment of
678 diabetic peripheral neuropathic pain. *BMC neurology* **9**, 6 (2009). https://doi.org/10.1186/1471-
679 2377-9-6
680 9 Callaghan, B. C., Cheng, H. T., Stables, C. L., Smith, A. L. & Feldman, E. L. Diabetic neuropathy:
681 clinical manifestations and current treatments. *Lancet Neurol* **11**, 521-534 (2012).
682 https://doi.org/10.1016/S1474-4422(12)70065-0
683 10 Finnerup, N. B. *et al.* Pharmacotherapy for neuropathic pain in adults: a systematic review and
684 meta-analysis. *Lancet Neurol* **14**, 162-173 (2015). https://doi.org/10.1016/S1474-4422(14)70251-
685 0
686 11 Attal, N. & Bouhassira, D. Advances in the treatment of neuropathic pain. *Curr Opin Neurol* **34**,
687 631-637 (2021). https://doi.org/10.1097/WCO.0000000000000980
688 12 Shinu, P. *et al.* Novel Therapies for the Treatment of Neuropathic Pain: Potential and Pitfalls. *J Clin*
689 *Med* **11** (2022). https://doi.org/10.3390/jcm11113002
690 13 Lauria, G. & Devigili, G. Skin biopsy as a diagnostic tool in peripheral neuropathy. *Nat Clin Pract*
691 *Neurol* **3**, 546-557 (2007). https://doi.org/10.1038/ncpneuro0630
692 14 Sommer, C. & Lauria, G. Skin biopsy in the management of peripheral neuropathy. *Lancet Neurol*
693 **6**, 632-642 (2007). https://doi.org/10.1016/S1474-4422(07)70172-2
694 15 Stucky, C. L. & Mikesell, A. R. Cutaneous pain in disorders affecting peripheral nerves. *Neuroscience*
695 *letters* **765**, 136233 (2021). https://doi.org/10.1016/j.neulet.2021.136233
696 16 Mikesell, A. R. *et al.* Keratinocyte PIEZO1 modulates cutaneous mechanosensation. *Elife* **11** (2022).
697 https://doi.org/10.7554/eLife.65987
698 17 Moehring, F. *et al.* Keratinocytes mediate innocuous and noxious touch via ATP-P2X4 signaling.
699 *Elife* **7** (2018). https://doi.org/10.7554/eLife.31684
700 18 Sadler, K. E., Moehring, F. & Stucky, C. L. Keratinocytes contribute to normal cold and heat
701 sensation. *Elife* **9** (2020). https://doi.org/10.7554/eLife.58625

19 Radtke, C., Vogt, P. M., Devor, M. & Kocsis, J. D. Keratinocytes acting on injured afferents induce extreme neuronal hyperexcitability and chronic pain. *Pain* **148**, 94-102 (2010). https://doi.org/10.1016/j.pain.2009.10.014

20 Talagas, M. *et al.* Keratinocytes Communicate with Sensory Neurons via Synaptic-like Contacts. *Annals of neurology* **88**, 1205-1219 (2020). https://doi.org/10.1002/ana.25912

21 Erbacher, C. *et al.* Interaction of human keratinocytes and nerve fiber terminals at the neuro-cutaneous unit. *Elife* **13** (2024). https://doi.org/10.7554/eLife.77761

22 van Niel, G., D'Angelo, G. & Raposo, G. Shedding light on the cell biology of extracellular vesicles. *Nat Rev Mol Cell Biol* **19**, 213-228 (2018). https://doi.org/10.1038/nrm.2017.125

23 Mathieu, M., Martin-Jaular, L., Lavieu, G. & Thery, C. Specificities of secretion and uptake of exosomes and other extracellular vesicles for cell-to-cell communication. *Nat Cell Biol* **21**, 9-17 (2019). https://doi.org/10.1038/s41556-018-0250-9

24 Gurung, S., Perocheau, D., Touramanidou, L. & Baruteau, J. The exosome journey: from biogenesis to uptake and intracellular signalling. *Cell Commun Signal* **19**, 47 (2021). https://doi.org/10.1186/s12964-021-00730-1

25 Kalluri, R. & LeBleu, V. S. The biology, function, and biomedical applications of exosomes. *Science* **367** (2020). https://doi.org/10.1126/science.aau6977

26 Pan, B. T., Teng, K., Wu, C., Adam, M. & Johnstone, R. M. Electron microscopic evidence for externalization of the transferrin receptor in vesicular form in sheep reticulocytes. *The Journal of cell biology* **101**, 942-948 (1985). https://doi.org/10.1083/jcb.101.3.942

27 Rastogi, S. *et al.* The Evolving Landscape of Exosomes in Neurodegenerative Diseases: Exosomes Characteristics and a Promising Role in Early Diagnosis. *Int J Mol Sci* **22** (2021). https://doi.org/10.3390/ijms22010440

28 Fan, Y., Chen, Z. & Zhang, M. Role of exosomes in the pathogenesis, diagnosis, and treatment of central nervous system diseases. *J Transl Med* **20**, 291 (2022). https://doi.org/10.1186/s12967-022-03493-6

29 Dai, J. *et al.* Exosomes: key players in cancer and potential therapeutic strategy. *Signal Transduct Target Ther* **5**, 145 (2020). https://doi.org/10.1038/s41392-020-00261-0

30 Lo Cicero, A. *et al.* Exosomes released by keratinocytes modulate melanocyte pigmentation. *Nature communications* **6**, 7506 (2015). https://doi.org/10.1038/ncomms8506

31 Nasiri, G., Azarpira, N., Alizadeh, A., Goshtasbi, S. & Tayebi, L. Shedding light on the role of keratinocyte-derived extracellular vesicles on skin-homing cells. *Stem Cell Res Ther* **11**, 421 (2020). https://doi.org/10.1186/s13287-020-01929-8

32 Zhou, X. *et al.* Exosome-Mediated Crosstalk between Keratinocytes and Macrophages in Cutaneous Wound Healing. *ACS Nano* **14**, 12732-12748 (2020). https://doi.org/10.1021/acsnano.0c03064

33 Jiang, M. *et al.* Keratinocyte exosomes activate neutrophils and enhance skin inflammation in psoriasis. *FASEB journal : official publication of the Federation of American Societies for Experimental Biology* **33**, 13241-13253 (2019). https://doi.org/10.1096/fj.201900642R

34 Kotzerke, K. *et al.* Immunostimulatory activity of murine keratinocyte-derived exosomes. *Exp Dermatol* **22**, 650-655 (2013). https://doi.org/10.1111/exd.12230

35 Ai, M. *et al.* Role of Human Mesenchymal Stem Cells and Derived Extracellular Vesicles in Reducing Sensory Neuron Hyperexcitability and Pain Behaviors in Murine Osteoarthritis. *Arthritis Rheumatol* **75**, 352-363 (2023). https://doi.org/10.1002/art.42353

36 Ashrafizadeh, M., Kumar, A. P., Aref, A. R., Zarrabi, A. & Mostafavi, E. Exosomes as Promising Nanostructures in Diabetes Mellitus: From Insulin Sensitivity to Ameliorating Diabetic Complications. *Int J Nanomedicine* **17**, 1229-1253 (2022). https://doi.org/10.2147/IJN.S350250

37 Sun, Y. *et al.* Human Mesenchymal Stem Cell Derived Exosomes Alleviate Type 2 Diabetes Mellitus by Reversing Peripheral Insulin Resistance and Relieving beta-Cell Destruction. *ACS Nano* **12**, 7613-7628 (2018). https://doi.org/10.1021/acsnano.7b07643

38 He, Q. *et al.* Mesenchymal stem cell-derived exosomes exert ameliorative effects in type 2 diabetes by improving hepatic glucose and lipid metabolism via enhancing autophagy. *Stem Cell Res Ther* **11**, 223 (2020). https://doi.org/10.1186/s13287-020-01731-6

39 Wei, P. *et al.* Exosomes derived from human amniotic epithelial cells accelerate diabetic wound healing via PI3K-AKT-mTOR-mediated promotion in angiogenesis and fibroblast function. *Burns Trauma* **8**, tkaa020 (2020). https://doi.org/10.1093/burnst/tkaa020

40 Fan, B. *et al.* Mesenchymal stromal cell-derived exosomes ameliorate peripheral neuropathy in a mouse model of diabetes. *Diabetologia* **63**, 431-443 (2020). https://doi.org/10.1007/s00125-019-05043-0

41 Ahmed, L. A. & Al-Massri, K. F. Exploring the Role of Mesenchymal Stem Cell-Derived Exosomes in Diabetic and Chemotherapy-Induced Peripheral Neuropathy. *Mol Neurobiol* (2024). https://doi.org/10.1007/s12035-024-03916-z

42 Jia, L. *et al.* Exosomes derived from high-glucose-stimulated Schwann cells promote development of diabetic peripheral neuropathy. *FASEB journal : official publication of the Federation of American Societies for Experimental Biology* **32**, fj201800597R (2018). https://doi.org/10.1096/fj.201800597R

43 Böing, A. N. *et al.* Single-step isolation of extracellular vesicles by size-exclusion chromatography. *J Extracell Vesicles* **3** (2014). https://doi.org/10.3402/jev.v3.23430

44 Arya, S. B., Collie, S. P. & Parent, C. A. The ins-and-outs of exosome biogenesis, secretion, and internalization. *Trends Cell Biol* **34**, 90-108 (2024). https://doi.org/10.1016/j.tcb.2023.06.006

45 Théry, C. *et al.* Minimal information for studies of extracellular vesicles 2018 (MISEV2018): a position statement of the International Society for Extracellular Vesicles and update of the MISEV2014 guidelines. *J Extracell Vesicles* **7**, 1535750 (2018). https://doi.org/10.1080/20013078.2018.1535750

46 Wang, Y. Z. *et al.* Notch receptor-ligand binding facilitates extracellular vesicle-mediated neuron-to-neuron communication. *Cell Rep* **43**, 113680 (2024). https://doi.org/10.1016/j.celrep.2024.113680

47 George, D. S. *et al.* Mitochondrial calcium uniporter deletion prevents painful diabetic neuropathy by restoring mitochondrial morphology and dynamics. *Pain* (2021). https://doi.org/10.1097/j.pain.0000000000002391

48 George, D. S. *et al.* The Mas-related G protein-coupled receptor d (Mrgprd) mediates pain hypersensitivity in painful diabetic neuropathy. *Pain* (2024). https://doi.org/10.1097/j.pain.0000000000003120

49 Jayaraj, N. D. *et al.* Reducing CXCR4-mediated nociceptor hyperexcitability reverses painful diabetic neuropathy. *The Journal of clinical investigation* **128**, 2205-2225 (2018). https://doi.org/10.1172/JCI92117

50 Menichella, D. M. *et al.* CXCR4 chemokine receptor signaling mediates pain in diabetic neuropathy. *Molecular pain* **10**, 42 (2014). https://doi.org/10.1186/1744-8069-10-42

51 Nowak, N. C., Menichella, D. M., Miller, R. & Paller, A. S. Cutaneous innervation in impaired diabetic wound healing. *Transl Res* **236**, 87-108 (2021). https://doi.org/10.1016/j.trsl.2021.05.003

52 Frühbeis, C. *et al.* Oligodendrocytes support axonal transport and maintenance via exosome secretion. *PLoS Biol* **18**, e3000621 (2020). https://doi.org/10.1371/journal.pbio.3000621

53 Graykowski, D. R., Wang, Y. Z., Upadhyay, A. & Savas, J. N. The Dichotomous Role of Extracellular Vesicles in the Central Nervous System. *iScience* **23**, 101456 (2020). https://doi.org/10.1016/j.isci.2020.101456

54 Greenhalgh, D. G. Wound healing and diabetes mellitus. *Clin Plast Surg* **30**, 37-45 (2003). https://doi.org/10.1016/s0094-1298(02)00066-4

55 Häger, S. C. & Nylandsted, J. Annexins: players of single cell wound healing and regeneration. *Commun Integr Biol* **12**, 162-165 (2019). https://doi.org/10.1080/19420889.2019.1676139

56 Creutz, C. E. The annexins and exocytosis. *Science* **258**, 924-931 (1992). https://doi.org/10.1126/science.1439804

57 Sønder, S. L. *et al.* Annexin A7 is required for ESCRT III-mediated plasma membrane repair. *Sci Rep* **9**, 6726 (2019). https://doi.org/10.1038/s41598-019-43143-4

58 Williams, J. K., Ngo, J. M., Lehman, I. M. & Schekman, R. Annexin A6 mediates calcium-dependent exosome secretion during plasma membrane repair. *Elife* **12** (2023). https://doi.org/10.7554/eLife.86556

59 Fan, B., Chopp, M., Zhang, Z. G. & Liu, X. S. Emerging Roles of microRNAs as Biomarkers and Therapeutic Targets for Diabetic Neuropathy. *Front Neurol* **11**, 558758 (2020). https://doi.org/10.3389/fneur.2020.558758

60 Ibrahim, H. M., AlZahrani, A., Hanieh, H., Ahmed, E. A. & Thirugnanasambantham, K. MicroRNA-7188-5p and miR-7235 regulates Multiple sclerosis in an experimental mouse model. *Mol Immunol* **139**, 157-167 (2021). https://doi.org/10.1016/j.molimm.2021.07.002

61 Mukherjee, S., Shelar, B. & Krishna, S. Versatile role of miR-24/24-1*/24-2* expression in cancer and other human diseases. *Am J Transl Res* **14**, 20-54 (2022).

62 Cui, M. *et al.* Interactive functions of microRNAs in the miR-23a-27a-24-2 cluster and the potential for targeted therapy in cancer. *J Cell Physiol* **235**, 6-16 (2020). https://doi.org/10.1002/jcp.28958

63 Lin, Z. *et al.* miR-24-3p Dominates the Proliferation and Differentiation of Chicken Intramuscular Preadipocytes by Blocking ANXA6 Expression. *Genes (Basel)* **13** (2022). https://doi.org/10.3390/genes13040635

64 Herrera, A. *et al.* Neurogenesis redirects β-catenin from adherens junctions to the nucleus to promote axonal growth. *Development* **150** (2023). https://doi.org/10.1242/dev.201651

65 Huang, Y. L. *et al.* Inhibition of Wnt/β-catenin signaling attenuates axonal degeneration in models of Parkinson's disease. *Neurochem Int* **159**, 105389 (2022). https://doi.org/10.1016/j.neuint.2022.105389

66 Duraikannu, A., Martinez, J. A., Chandrasekhar, A. & Zochodne, D. W. Expression and Manipulation of the APC-β-Catenin Pathway During Peripheral Neuron Regeneration. *Sci Rep* **8**, 13197 (2018). https://doi.org/10.1038/s41598-018-31167-1

67 Lewallen, K. A. *et al.* Assessing the role of the cadherin/catenin complex at the Schwann cell-axon interface and in the initiation of myelination. *The Journal of neuroscience : the official journal of the Society for Neuroscience* **31**, 3032-3043 (2011). https://doi.org/10.1523/jneurosci.4345-10.2011

68 Alto, L. T. & Terman, J. R. Semaphorins and their Signaling Mechanisms. *Methods in molecular biology* **1493**, 1-25 (2017). https://doi.org/10.1007/978-1-4939-6448-2_1

69 Janssen, B. J. *et al.* Structural basis of semaphorin-plexin signalling. *Nature* **467**, 1118-1122 (2010). https://doi.org/10.1038/nature09468

70 Takamatsu, H. & Kumanogoh, A. Diverse roles for semaphorin-plexin signaling in the immune system. *Trends in immunology* **33**, 127-135 (2012). https://doi.org/10.1016/j.it.2012.01.008

71 Li, Y. *et al.* Macrophages facilitate peripheral nerve regeneration by organizing regeneration tracks through Plexin-B2. *Genes Dev* **36**, 133-148 (2022). https://doi.org/10.1101/gad.349063.121

72 Paldy, E. *et al.* Semaphorin 4C Plexin-B2 signaling in peripheral sensory neurons is pronociceptive in a model of inflammatory pain. *Nature communications* **8**, 176 (2017). https://doi.org/10.1038/s41467-017-00341-w

73 Li, J., Liu, H. Q., Li, X. B., Yu, W. J. & Wang, T. Function of Adenosine 2A Receptor in High-Fat Diet-Induced Peripheral Neuropathy. *J Diabetes Res* **2020**, 7856503 (2020). https://doi.org/10.1155/2020/7856503

74 Kopan, R. & Ilagan, M. X. The canonical Notch signaling pathway: unfolding the activation mechanism. *Cell* **137**, 216-233 (2009). https://doi.org/10.1016/j.cell.2009.03.045

75 Zhang, Y., Lowe, S., Ding, A. Z. & Li, X. Notch-dependent binary fate choice regulates the Netrin pathway to control axon guidance of Drosophila visual projection neurons. *Cell Rep* **42**, 112143 (2023). https://doi.org/10.1016/j.celrep.2023.112143

76 Sullivan, J. M. *et al.* Dominant mutations of the Notch ligand Jagged1 cause peripheral neuropathy. *The Journal of clinical investigation* **130**, 1506-1512 (2020). https://doi.org/10.1172/jci128152

77 Wolfes, A. C. & Dean, C. The diversity of synaptotagmin isoforms. *Curr Opin Neurobiol* **63**, 198-209 (2020). https://doi.org/10.1016/j.conb.2020.04.006

78 Ullah, N., Maaiden, E. E., Uddin, M. S. & Ashraf, G. M. Synaptotagmin-1: A Multi-Functional Protein that Mediates Vesicle Docking, Priming, and Fusion. *Curr Protein Pept Sci* **22**, 470-478 (2021). https://doi.org/10.2174/1389203722666210325110231

79 Thiel, G. Synapsin I, synapsin II, and synaptophysin: marker proteins of synaptic vesicles. *Brain pathology* **3**, 87-95 (1993). https://doi.org/10.1111/j.1750-3639.1993.tb00729.x

80 Cesca, F., Baldelli, P., Valtorta, F. & Benfenati, F. The synapsins: key actors of synapse function and plasticity. *Progress in neurobiology* **91**, 313-348 (2010). https://doi.org/10.1016/j.pneurobio.2010.04.006

81 Park, D. *et al.* Cooperative function of synaptophysin and synapsin in the generation of synaptic vesicle-like clusters in non-neuronal cells. *Nature communications* **12**, 263 (2021). https://doi.org/10.1038/s41467-020-20462-z

82 Talagas, M. Anatomical contacts between sensory neurons and epidermal cells: an unrecognized anatomical network for neuro-immuno-cutaneous crosstalk. *Br J Dermatol* **188**, 176-185 (2023). https://doi.org/10.1093/bjd/ljac066

83 Vieira, W. F. *et al.* Anti-hyperalgesic effects of photobiomodulation therapy (904 nm) on streptozotocin-induced diabetic neuropathy imply MAPK pathway and calcium dynamics modulation. *Sci Rep* **12**, 16730 (2022). https://doi.org/10.1038/s41598-022-19947-2

84 Aghaee-Bakhtiari, S. H. *et al.* MAPK and JAK/STAT pathways targeted by miR-23a and miR-23b in prostate cancer: computational and in vitro approaches. *Tumour Biol* **36**, 4203-4212 (2015). https://doi.org/10.1007/s13277-015-3057-3

85 Perdas, E., Stawski, R., Nowak, D. & Zubrzycka, M. The Role of miRNA in Papillary Thyroid Cancer in the Context of miRNA Let-7 Family. *Int J Mol Sci* **17** (2016). https://doi.org/10.3390/ijms17060909

86 Wang, S. *et al.* MicroRNA-24 in Cancer: A Double Side Medal With Opposite Properties. *Front Oncol* **10**, 553714 (2020). https://doi.org/10.3389/fonc.2020.553714

87 Lin, Y. *et al.* miR-24-3p stimulates migration, invasion and proliferation of prostate cancer cells by targeting suppressor of cytokine signaling 6. *Int J Clin Exp Pathol* **11**, 1803-1810 (2018).

88 Xiang, Y. miR-24 in diabetes. *Oncotarget* **6**, 16816-16817 (2015). https://doi.org/10.18632/oncotarget.4795

89 George, D. S. *et al.* A subpopulation of peripheral sensory neurons expressing the Mas-related G Protein-Coupled Receptor d (Mrgprd) generates pain hypersensitivity in painful diabetic neuropathy. *bioRxiv*, 2022.2010.2027.514066 (2022). https://doi.org/10.1101/2022.10.27.514066

90 George, D. S. *et al.* The Mas-related G protein-coupled receptor d (Mrgprd) mediates pain hypersensitivity in painful diabetic neuropathy. *Pain* (2023). https://doi.org/10.1097/j.pain.0000000000003120

892 91 Asadi, J. *et al.* Enhanced imaging of lipid rich nanoparticles embedded in methylcellulose films for
893 transmission electron microscopy using mixtures of heavy metals. *Micron* **99**, 40-48 (2017).
894 https://doi.org/10.1016/j.micron.2017.03.019
895 92 Menichella, D. M. *et al.* Ganglioside GM3 synthase depletion reverses neuropathic pain and small
896 fiber neuropathy in diet-induced diabetic mice. *Molecular pain* **12** (2016).
897 https://doi.org/10.1177/1744806916666284
898 93 Eng, J. K., McCormack, A. L. & Yates, J. R. An approach to correlate tandem mass spectral data of
899 peptides with amino acid sequences in a protein database. *J Am Soc Mass Spectrom* **5**, 976-989
900 (1994). https://doi.org/10.1016/1044-0305(94)80016-2
901 94 Xu, T. *et al.* ProLuCID: An improved SEQUEST-like algorithm with enhanced sensitivity and
902 specificity. *J Proteomics* **129**, 16-24 (2015). https://doi.org/10.1016/j.jprot.2015.07.001
903 95 Cociorva, D., D, L. T. & Yates, J. R. Validation of tandem mass spectrometry database search results
904 using DTASelect. *Curr Protoc Bioinformatics* **Chapter 13**, Unit 13.14 (2007).
905 https://doi.org/10.1002/0471250953.bi1304s16
906 96 Tabb, D. L., McDonald, W. H. & Yates, J. R., 3rd. DTASelect and Contrast: tools for assembling and
907 comparing protein identifications from shotgun proteomics. *J Proteome Res* **1**, 21-26 (2002).
908 https://doi.org/10.1021/pr015504q
909 97 UniProt: a hub for protein information. *Nucleic Acids Res* **43**, D204-212 (2015).
910 https://doi.org/10.1093/nar/gku989
911 98 Chen, Y. & Wang, X. miRDB: an online database for prediction of functional microRNA targets.
912 *Nucleic Acids Res* **48**, D127-d131 (2020). https://doi.org/10.1093/nar/gkz757